Computational analysis of the core refractive index dependencies of Brillouin frequency shift and Brillouin power change in Brillouin coherent detection based distributed sensing systems

ABDURRAHMAN GÜNDAY[*]

Program of Electronics Technology, Vocational School of Orhangazi Yeniköy Asil Çelik, Uludağ University, 16800 Orhangazi, Bursa, Turkey

Brillouin frequency shift (BFS) and Brillouin power change (BPC) and the core refractive index of the sensing fiber vary linearly with thermal formations in the medium. In this study, a novel Brillouin Coherent detection based distributed temperature and thermal strain sensing model depending on the core refractive index dependencies of BFS and BPC has been proposed. Using this model, core refractive index dependencies of BFS and BPC have been theoretically analyzed and corresponding simulations have been performed, accordingly. In this research, for 20 °C – 39.44 °C temperature range of the sensing fiber, refractive index of the fiber core changes from 1.44183 to 1.44202. Moreover, BFS and BPC values along the sensing fiber have been obtained as 43.80 MHz, 62.05 MHz and 66.92 MHz and 10.44 %, 13.04 % and 13.73 % versus core refractive index values of 1.44193, 1.44200 and 1.44202, respectively. Nevertheless, RMS error values of BFS and BPC have been computed for specific fiber regions along the sensing fiber and then using the interpolation method, linear and quadratic equations of the RMS curves have been derived. According to the results of the simulations and the equations, average values of the frequency and power RMS have been attained as ~ 1.60 MHz and ~ 0.26 %, respectively. Furthermore, quadratic equations related to the core refractive index dependencies of Brillouin parameters and the cubic equations relative to the temperature and thermal strain resolutions of the system have been produced by utilizing interpolation and curve fitting methods. Consequently, temperature and thermal strain resolutions of the system have been calculated as ~ 0.76 °C and ~ 46.80 με for the entire length of the sensing fiber, respectively.

1. Introduction

Physical formations such as temperature, strain and vibration are generally measured by using power, frequency and phase changes of the backscattered light in the optical fiber distributed sensing systems. In these sensing systems whilst the Rayleigh scattering based phase-sensitive OTDR (Optical Time Domain Reflectometry) technique is widely used for detecting vibration and acoustic wave formations [1-4], spontaneous Brillouin scattering based BODTR (Brillouin Optical Time Domain Reflectometry) technique is utilized for measuring temperature and thermal strain formations simultaneously [5, 6].

In Rayleigh scattering based phase-sensitive OTDR technique which in principle is similar to conventional OTDR, a pulse of the light is launched into the sensing fiber and then backscattered Rayleigh signal is measured depending on the phase change induced by strain variations between two different regions on the fiber. In other words, this technique is based on measuring the phase difference which is directly related to the changes in

strain or acoustic vibration between two different points of the sensing fiber [2].

BOTDR technique is based on spontaneous Brillouin scattering where backscattered light is captured from the sensing fiber and then detected its peak frequency, as well. In other words, BOTDR makes use of spontaneous Brillouin scattering which is exploited for perceiving the frequency shift between backscattered light and the incident light pumped into the fiber. This frequency shift, i.e. BFS is highly proportional to the ambient temperature and thermal strain formations [7].

In the sensing system which is based on spontaneous Brillouin scattering, there are two distinct methods utilized for getting information related to the temperature and thermal strain formations, called Direct Detection Method (DDM) and Coherent Detection Method (CDM).

In direct detection of spontaneous Brillouin scattering, since the thermal strain effects on Brillouin power are neglected, Brillouin power is only used for measuring temperature variations along the sensing fiber. Thus, the BFS information is not required. In this method, optical filtering is utilized to separate the Brillouin signal from the Rayleigh signal and LPR (Landau-Placzek ratio) is used

for getting the absolute temperature information along the fiber [8]. In such a sensing system where DDM is used for measuring the temperature and thermal strain formations simultaneously, Mach-Zehnder interferometer is widely utilized. On the contrary, DDM has limitations with regards to sensing range of the system and accuracy of the measurements [9].

In CDM, simultaneous measurements of temperature and thermal strain variations can easily be provided by using BFS and BPC. This method in principle is based on mixing optical Local Oscillator (LO) signal with backscattered signal and producing the beat frequency of ~ 11 GHz via Fiber Bragg Grating (FBG). FBG used in CDM allows the Rayleigh (R) and Brillouin Stokes (BS) components to be transmitted and reflects the Brillouin anti-Stokes (BAS) component to be mixed with LO signal. Afterwards, the Brillouin spectrum along the sensing fiber is built from the time-domain traces and thus the temperature and thermal strain variations are detected by Coherent detection system [8].

For long range (> 10 km) Brillouin Coherent detection based distributed sensing systems, maximizing the weak Brillouin backscattered signal is crucial, since it specifies sensing performance of the system. Therefore, it is necessary to achieve an improvement on the Brillouin backscattered power to provide longer sensing range and better sensing performance [8], despite the fact that Coherent based sensing systems generally depend on stimulated Brillouin scheme. However, since a 3 km length of the sensing fiber is utilized in this study, spontaneous Brillouin scheme is employed to minimize the attenuation effect along the fiber. Moreover, in this research, a distributed sensing model based on the combined effect of the fiber core refractive index and the Coherent detection of spontaneous Brillouin scattering has been exploited for making theoretical analysis and getting corresponding simulations.

Furthermore, simultaneous temperature and thermal strain measurements and the RMS error values along the fiber are obtained by using the core refractive index dependencies of Brillouin parameters, i.e. BFS and BPC in the model illustrated in Fig. 1. In this model, a pulsed laser source with the output power of 1.5 mW operating at 1550 nm is used as optical pulse producer. Optical pulses generated by the pulsed laser source are amplified using Erbium doped fiber amplifiers EDFA1 and EDFA2 and then launched into the sensing fiber. EDFAs utilized for optical amplification provide up to ~ 3 dB overall improvement on the backscattered Brillouin power. Fiber coupler FC2 used in the model is employed to direct the optical pulses to the heating units located on different fiber regions. The heating units having distinctive thermal capacities are exploited for producing thermal effects into the sensing fiber. Since the thermally generated acoustic waves in the sensing fiber interact with incident light waves of the optical pulses pumped into the fiber, optical pulses are scattered back in the waveguide and thus, spontaneous Brillouin scattering occurs. The backscattered optical signal includes Brillouin Stokes, Rayleigh and Brillouin anti-Stokes components. Optic components of

the backscattered signal are routed towards the EDFA3 amplifier via fiber coupler FC2 at the same time. Since the ASE (amplified spontaneous emission) noise can exist at the output end of the amplifier, an acousto-optic modulator AOM is used to gate the ASE noise in the model. In this manner, it is aimed to increase the SNR (signal to noise ratio) by employing filtering technique which eliminates the noise added on the Brillouin backscattered signal. Optical circulator OC used in the model is utilized for directing the optical signal involving BS, R and BAS components towards the Fiber Bragg Grating (FBG). FBG is a kind of optical reflector which reflects particular wavelength (λ_g) of optical signal and transmits all others in the frequency spectrum [10]. In the model, FBG allows Rayleigh (R) and Brillouin Stokes (BS) components to be transmitted towards the local oscillator (LO), whilst reflecting Brillouin anti-Stokes (BAS) component back to the optical circulator. The local oscillator signal (LO) produced by LO is mixed with BAS signal then routed towards the Coherent detection system via optical circulator. Afterwards, detection system transmits the mixed signal with a value of 11.09 GHz to be detected by a photodetector and then it is directed towards the PC analyzer and Oscilloscope to be analyzed and monitored.
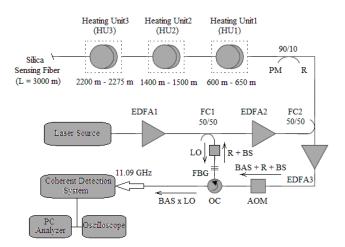

Fig. 1. Brillouin Coherent Detection based distributed temperature and thermal strain sensing model

In distributed sensing systems similar to the model in Fig. 1, determining the overall measurement time affecting sensing performance is crucial [8] and highly essential to be known, since the distributed sensing systems are mostly used in real time and a pseudo real time measurement of parameters such as temperature, strain and vibration formations. The total measurement time generally depends on frequency range, frequency step, number of averages, length of the sensing fiber and data acquisition system consists of Coherent detection system, PC analyzer and oscilloscope. In order to determine the total measurement time of the system, frequency range requires to be estimated carefully in order to avoid collecting time-domain traces of unnecessary frequencies [8]. For the model in Fig. 1, a frequency range of about 20 MHz provides good accuracy to measure temperature and

thermal strain formations, due to the operating temperature of the sensing fiber changes in the range of few centigrade degrees. Another factor affecting the sensing performance of the system is frequency step which means frequency interval between consecutive measured frequencies. Frequency step can be chosen around 5 MHz in order to reduce the measurement time. For the optimum values of frequency range and frequency step, i.e. 20 MHz and 5 MHz, respectively, 4 time-domain traces need to be measured. Since the each time-domain trace is generally averaged 2^{12} times, it takes ~ 50 s. The sensing fiber utilized in this study is 3 km, hence the round trip time is computed as ~ 30 μs. Since the total transfer time of the detection system and PC analyzer is around few seconds, overall measurement time is obtained as about few minutes. This is considerable value of total measurement time of Brillouin Coherent detection based distributed sensing model configured in Fig. 1.

2. Temperature and thermal strain dependencies of fiber core refractive index

Refractive index of any material is a distinctive characteristic such as density, melting points, thermal resistance and Poisson's ratio. When the refractive index of a material is measured, it is possible to get meaningful information about the specification of the matter.

Core refractive index of the sensing fiber used in distributed sensing systems is affected by thermal variations occurred in the medium due to its temperature dependency. Bansal and Doremus observed in their investigation that the refractive index of fused silica changed linearly with the ambient temperature in range of 200 °K – 1000 °K [11].

Temperature dependence of the core refractive index of the sensing fiber is given as

$$n(T_K) = 1.4389 + 1 \times 10^{-5} T_K \qquad (1)$$

where T_K is temperature in Kelvin [12].

Using the formulas related to temperature and thermal strain dependencies of Young's modulus of the sensing fiber core $E_{T_K} = 69.68 + 1.126 \times 10^{-2} T_K$ and $E_\varepsilon = E_0(1 + 5.75\,\varepsilon)$ respectively [12, 13, 14], temperature dependence of the thermal strain formations can be written by

$$\varepsilon = 26.83314 T_K - 7862.111 \qquad (2)$$

where E_{T_K} and E_ε are Young's modulus variations with respect to temperature and thermal strain in GPa, respectively, E_0 is the Young's modulus at zero strain and 293 °K temperature, i.e. 72.97918 GPa, ε is the thermal strain in terms of μɛ.

Benefiting from (1) and (2), thermal strain dependence of core refractive index of the sensing fiber is given in (3).

$$n(\varepsilon) = 1.44183 + 3.726735 \times 10^{-7} \varepsilon \qquad (3)$$

Temperature and thermal strain dependencies of the core refractive index of the sensing fiber in ranges of 200 °K – 1000 °K and 0 μɛ – 18971 μɛ are shown in Figs. 2a and 2b, respectively. As seen in Figs. 2a and 2b, core refractive index of the sensing fiber varies linearly with temperature and thermal strain variations.
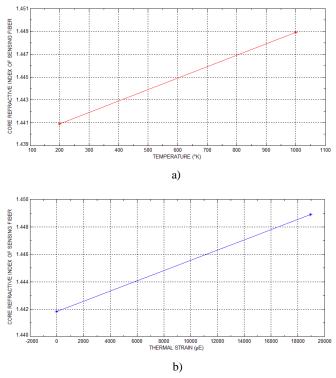

a)

b)

Fig. 2. a) Temperature and b) thermal strain dependencies of core refractive index of the sensing fiber

3. Fiber core refractive index dependencies of Brillouin frequency shift and Brillouin power change

Brillouin frequency shifts $V_B(T)$ and $V_B(\varepsilon)$ induced by temperature and thermal strain formations occurred along the sensing fiber are given as

$$V_B(T) = V_B(T_r)[1 + K_T(T - T_r)] \qquad (4.a)$$

$$V_B(\varepsilon) = V_B(0)[1 + K_\varepsilon(\varepsilon - 0)] \qquad (4.b)$$

respectively [15, 16, 5, 7], where $V_B(T_r)$ is the BFS at T_r reference temperature, T is the temperature of the sensing fiber in terms of °K, $V_B(0)$ is the BFS at zero thermal strain, K_T and K_ε are the temperature and strain coefficients, respectively [15].

Temperature and thermal strain coefficients K_T^V and K_ε^V governing Brillouin frequency shifts are expressed in (5.a) and (5.b), respectively [12].

$$K_T^V(T) = K_T V_B(T_r) \qquad (5.a)$$

$$K_\varepsilon^V(\mu\varepsilon) = K_\varepsilon V_B(0) \qquad (5.b)$$

Making use of (4) and (5), Brillouin frequency shifts $\Delta V_B(T)$ and $\Delta V_B(\varepsilon)$ depending on temperature and thermal strain formations can be written as given in (6.a) and (6.b), respectively.

$$\Delta V_B(T) = K_T^V(T - T_r) \tag{6.a}$$

$$\Delta V_B(\varepsilon) = K_\varepsilon^V(\varepsilon - 0) \tag{6.b}$$

Unifying (6.a) and (6.b), BFS is rewritten as a function of temperature and thermal strain variations in form of (7).

$$\Delta V_B(T, \varepsilon) = K_T^V \Delta T + K_\varepsilon^V \Delta \varepsilon \tag{7}$$

Brillouin power changes $P_B(T)$ ve $P_B(\varepsilon)$ caused by temperature and thermal strain formations occurred along the sensing fiber are given by [12]

$$P_B(T) = P_B(T_r)[1 + K_T(T - T_r)] \tag{8.a}$$

$$P_B(\varepsilon) = P_B(0)[1 + K_\varepsilon(\varepsilon - 0)] \tag{8.b}$$

where $P_B(T_r)$ and $P_B(0)$ are the BPC at T_r reference temperature, respectively and $P_B(0)$ is the BPC at zero thermal strain [12, 15].

Temperature and thermal strain coefficients of the Brillouin power changes K_T^P and K_ε^P are expressed in (9.a) and (9.b), respectively [12].

$$K_T^P(T) = K_T P_B(T_r) \tag{9.a}$$

$$K_\varepsilon^P(\mu\varepsilon) = K_\varepsilon P_B(0) \tag{9.b}$$

The temperature and strain coefficients of BFS and BPC for single-mode fiber (SMF) are given in Table 1 [8, 17].

Table 1. Temperature and strain coefficients for SMF

Coefficients	Corresponding Values
K_T^V	1.07 ± 0.06 MHz/(°C)
K_ϵ^V	0.048 ± 0.004 MHz/($\mu\varepsilon$)
K_T^P	0.36 ± 0.030 %/(°C)
K_ϵ^P	$-9\times10^{-4} \pm 1\times10^{-5}$ %/($\mu\varepsilon$)

Using (8) and (9), Brillouin power changes $\Delta P_B(T)$ and $\Delta P_B(\varepsilon)$ can be written as a function of temperature and thermal strain formations as given in (10.a) and (10.b), respectively.

$$\Delta P_B(T) = K_T^P(T - T_r) \tag{10.a}$$

$$\Delta P_B(\varepsilon) = K_\varepsilon^P(\varepsilon - 0) \tag{10.b}$$

Unifying (10.a) and (10.b), temperature and thermal strain dependencies of BPC can be rewritten as in (11).

$$\Delta P_B(T, \varepsilon) = K_T^P \Delta T + K_\varepsilon^P \Delta \varepsilon \tag{11}$$

Converting the temperature term from °K to °C in (1), the core refractive index is expressed as a function of the temperature as

$$T_C = 1\text{x}10^5 n(T_C) - 1.44163\text{x}10^5 \tag{12}$$

where T_C is the temperature formations occurred along the sensing fiber in terms of °C.

Utilizing (3), thermal strain formations depending on the changes of core refractive index can be written as in (13).

$$\varepsilon = 26.83314\text{x}10^5 n(\varepsilon) - 38.68883\text{x}10^5 \tag{13}$$

Generalizing (7) and (11), ΔV_B and ΔP_B emerged along the entire length of the sensing fiber can be achieved as in (14) and (15), respectively.

$$\Delta V_B(L) = K_T^V T_C(L) + K_\varepsilon^V \varepsilon(L) \tag{14}$$

$$\Delta P_B(L) = K_T^P T_C(L) + K_\varepsilon^P \varepsilon(L) \tag{15}$$

ΔV_B and ΔP_B can be expressed as a function of the core refractive index in matrix form as in (16).

$$\begin{bmatrix} \Delta V_B(n) \\ \Delta P_B(n) \end{bmatrix} = \begin{bmatrix} K_T^V & K_\varepsilon^V \\ K_T^P & K_\varepsilon^P \end{bmatrix} \begin{bmatrix} T_C(n) \\ \varepsilon(n) \end{bmatrix} \tag{16}$$

Substituting (12) and (13) and the temperature and strain coefficients given in Table 1 in (16) and reorganizing the equation, core refractive index dependencies of BFS and BPC are obtained as given in (17.a) and (17.b), respectively.

$$\Delta V_B(n) = 2.35799 \text{ x } 10^5 n - 3.39961 \text{ x } 10^5 \tag{17.a}$$

$$\Delta P_B(n) = 0.3358502 \text{ x } 10^5 n - 0.48416685 \text{ x } 10^5 \tag{17.b}$$

The absolute value of the determinant of 2x2 square matrix related to the temperature and thermal strain coefficients given in (16) is crucial, since it specifies the temperature and thermal strain resolutions so as to evaluate sensing performance of the systems. In other words, the larger the absolute value of the determinant, the smaller the computed resolutions of the system [8, 12].

Temperature resolution δ_T and thermal strain resolution δ_ϵ of any Brillouin based distributed sensing system are computed with

$$\delta_T = \frac{|K_\epsilon^P \delta V| + |K_\epsilon^V \delta P|}{|K_T^V \cdot K_\varepsilon^P - K_\varepsilon^V \cdot K_T^P|} \tag{18.a}$$

$$\delta_\varepsilon = \frac{|K_T^P \delta V| + |K_T^V \delta P|}{|K_T^V \cdot K_\varepsilon^P - K_\varepsilon^V \cdot K_T^P|} \tag{18.b}$$

respectively [8, 12], where δV and δP are RMS error values relative to the RMS noises occurred on BFS and BPC, respectively.

Parameters of δV and δP given in (18.a) and (18.b) also denote the Brillouin frequency and Brillouin power resolutions, as well.

4. Simulations

Simulations corresponding with the computational analysis of the core refractive index dependencies of Brillouin parameters for the model based on the Coherent detection of spontaneous Brillouin scattering have been carried out using Matlab.

All parameters of the sensing fiber and the characteristics of laser source used for getting simulations are highlighted as follows: refractive indices of the silica optical fiber core and cladding (n_1 and n_2) are 1.44183 and 1.43, respectively, capturing coefficient ($S = (n_1^2 - n_2^2)/4n_1^2$) is 4.0856×10^{-3}, photoelastic or Pockel coefficient (p) is 0.286, Boltzmann's constant (k) is 1.38×10^{-23} J/K, wavelength of the optical signal (λ) is 1550 nm, density of the silica fiber (ρ) is 2330 kg/m³, acoustic velocity in the glass (v_a) is 5960 m/s, maximum output power of the optical signal pumped by the pulsed laser source (P_0) is 1.5 mW, operating wavelength of the pulsed laser source is 1550 nm, pulse duration of the optical signal pumped by the laser (τ) is 11 ns, Brillouin and Rayleigh scattering coefficients at 1550 nm (γ_B and γ_R) are $1.0691 \times 10^{-6} \, \text{m}^{-1}$ and $34.108 \times 10^{-6} \, \text{m}^{-1}$, respectively, speed of the light in vacuum (c) is 2.99793×10^8 m/s, group velocity of the light propagating in the fiber ($v_g = c/n_1$) is 2.08×10^8 m/s, spatial resolution ($l = c\tau/2n_1$) is 1.1436 m, length of the sensing fiber (L) is 3000 m, number of the measurement points along the fiber (R = L/l) is 2623.

Locations of the heating units positioned along the sensing fiber are given in Table 2.

Table 2. Locations of the heating units along the sensing fiber

Heating Units	Fiber Locations
HU1	600 m – 650 m
HU2	1400 m – 1500 m
HU3	2200 m – 2275 m

BFS and BPC profiles are schematically illustrated in Figs. 3a and 3b, respectively.
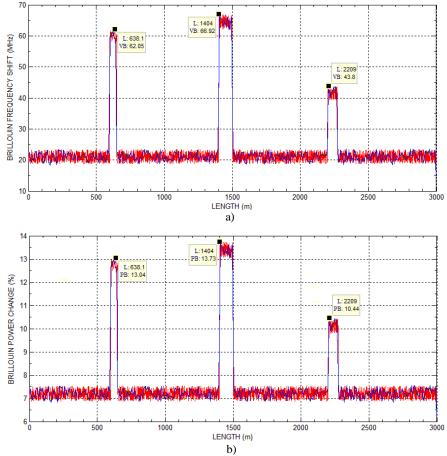

a)

b)

Fig. 3. a) BFS and b) BPC profiles along the sensing fiber

BFS reaches its maximum value of 66.92 MHz in the fiber region where sensing fiber is passing through the heating unit HU2. In the fiber regions where the sensing fiber is passing through the heating units HU1 and HU3, BFS gets the values of 62.05 MHz and 43.80 MHz at the 638th and the 2209th meters of the fiber, respectively. BPC takes its greatest value of 13.73 % at the 1404th meter of the fiber. In the fiber regions on where HU1 and HU2 are located, it has power peaks with the values of 13.04 % and 10.44 % at the 638th and the 2209th meters of the fiber, respectively. In other regions of the sensing fiber, BFS and BPC get average values with ~ 21.072 MHz and ~ 7.204 % as shown in Figs. 3a and 3b. Temperature profile is shown in Fig. 4.
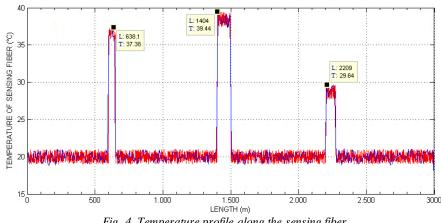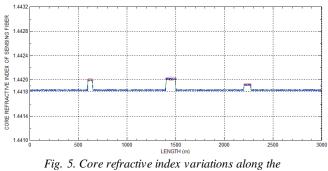

Fig. 4. Temperature profile along the sensing fiber

As shown in Fig. 4, the temperature peaks are obtained on the fiber regions where the Brillouin peaks exist, accordingly.

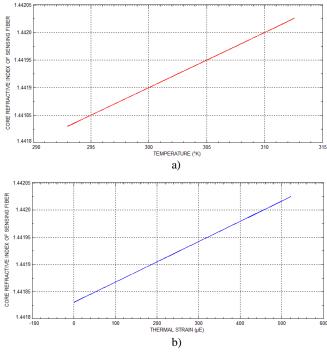The core refractive index variation along the sensing fiber is illustrated in Fig. 5.

Fig. 5. Core refractive index variations along the sensing fiber

Since the core refractive index changes linearly with thermal effects occurred in the medium, it gets maximum values in the fiber regions where the greatest temperature values are reached. For the maximum temperature value of 39.44 °C at the 1404th meter of the sensing fiber, core refractive index value is attained as 1.44202. In the fiber regions where it is passing through the heating units HU1 and HU3, core refractive index reaches the values of 1.44200 and 1.44193, respectively.

The simulations in concern with the core refractive index variations in ranges of 20 °C – 39.44 °C and 0 με – 521.635 με are shown in Figs. 6a and 6b, respectively. As seen in the Figs. 6a and 6b, it changes linearly with temperature and thermal strain formations.

Using simulations given in Figs. 3a and 3b, RMS error values of BFS and BPC are computed for eight different fiber regions as given in Table 3. Furthermore, the plots representing both linear and quadratic forms of the equation related to Brillouin frequency shift RMS and Brillouin power change RMS are obtained along the sensing fiber as shown in Figs. 7a and 7b, respectively.

a)

b)

Fig. 6. Variation of the core refractive index with a) temperature and b) thermal strain formations

As seen obviously in the plots shown in Figs. 7a and 7b, the quadratic equations give the optimum results for computing RMS error values in comparison to the linear

equations and overlap with the corresponding values. According to RMS errors values in Table 3, linearity for the Figs. 7a and 7b are acquired as 97.40 % and 96.11 %, respectively. These values are meaningful and provide good matching with the values marked on plots in Figs. 7a and 7b.

Linear and quadratic equations in concern with the RMS error values of the Brillouin parameters are derived by using interpolation method. Both the linear and quadratic equations of Brillouin frequency shift RMS and Brillouin power change RMS can be expressed as a function of the sensing fiber length as

$$RMS_V = 2.9159x10^{-4}L + 1.1396 \quad (19.a)$$

$$RMS_V = -4.2681x10^{-8}L^2 + 4.2677x10^{-4}L + 1.0645 \quad (19.b)$$

$$RMS_P = 3.9887x10^{-5}L + 0.19543 \quad (20.a)$$

$$RMS_P = -1.4236x10^{-8}L^2 + 8.4975x10^{-5}L + 0.17038 \quad (20.b)$$

respectively, where RMS_V and RMS_P are Brillouin frequency shift RMS and Brillouin power change RMS, respectively, and L is length of the sensing fiber. RMS_V and RMS_P given in (19) and (20) denote the Brillouin frequency resolution (δV) and Brillouin power resolution (δP) specified in (18).
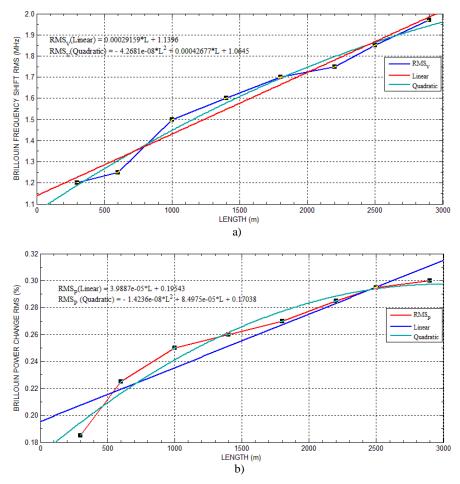

Fig. 7. a) Brillouin frequency shift RMS and b) Brillouin power change RMS

Using RMS error values obtained from the curves in Figs. 7a and 7b and temperature and strain coefficients given in Table 1, temperature resolution Res_T (δ_T) and thermal strain resolution Res_S ($\delta\varepsilon$) are computed for eight different locations along the sensing fiber and corresponding plots are shown as in Figs. 8a and 8b, respectively.

It can be clearly seen from Figs. 8a and 8b that the curves representing temperature and thermal strain resolutions are similar to the curves of Brillouin frequency and power RMS shown in Figs. 7a and 7b, respectively. This result indicates that the noises occurred on BFS and

BPC are responsible for thermal strain resolution and temperature resolution, accordingly.

Utilizing the interpolation and curve fitting methods, cubic equations of temperature and thermal strain resolution are derived as a function of the sensing fiber length as in (21.a) and (21.b), respectively.

$$Res_T = 3x10^{-11}L^3 - 1.9x10^{-7}L^2 + 0.44x10^{-3}L + 0.44 \quad (21.a)$$

$$Res_S = 1.362x10^{-9}L^3 - 8.235x10^{-6}L^2 + 0.02219L + 28.19 \quad (21.b)$$

Using (18.a), (18.b) and simulation results, RMS error values and temperature and thermal strain resolutions are calculated for specific fiber regions as given in Table 3.

Table 3. RMS error values and temperature and thermal strain resolutions for specific fiber regions

Fiber Regions (m)	RMS_V (MHz)	RMS_P (%)	Res_T (°C)	Res_S (µε)
300 m - 400 m	1.20	0.185	0.55	34.53
600 m - 650 m	1.25	0.225	0.65	37.86
1000 m - 1100 m	1.50	0.250	0.73	44.26
1400 m - 1500 m	1.60	0.260	0.76	46.82
1800 m - 1900 m	1.70	0.270	0.79	49.38
2200 m - 2275 m	1.75	0.285	0.84	51.25
2500 m - 2600 m	1.85	0.295	0.87	53.81
2900 m - 2975 m	1.97	0.300	0.89	56.47

Using resolution values given in Table 3, linearity for the Figs. 8a and 8b are achieved as 97.23 % and 99.34 %, respectively. It means that the curves of the temperature and thermal strain resolutions highly overlap with the corresponding values. Using Table 3, average values of

Brillouin frequency and power RMS have been attained as ~ 1.60 MHz and ~ 0.26 %, respectively.

Moreover, temperature and thermal strain resolutions of Brillouin Coherent detection based sensing model given in Fig. 1 are computed as ~ 0.76 °C and ~ 46.80 µε, respectively. Core refractive index dependencies of BFS and BPC are shown in Figs. 9 and 10, respectively.

Using the simulation results given in Figs. 9 and 10, quadratic equations in concern with the core refractive index dependencies of the Brillouin parameters are derived as in (22.a) and (22.b), respectively.

$$\Delta V_B(n) = -87.703x10^{-5}n^2 + 2.358x10^5 n - 3.3996x10^5 \quad (22.a)$$

$$\Delta P_B(n) = -1.21x10^{-4}n^2 + 3.359x10^4 n - 4.842x10^4 \quad (22.b)$$

It is obviously seen that the equations given in (22.a) and (22.b) are in agreement with those in (17.a) and (17.b), respectively. However, quadratic forms of the equations are more useful in comparison with linear forms of the equations so as to get values of the core refractive index and Brillouin parameters along the sensing fiber.
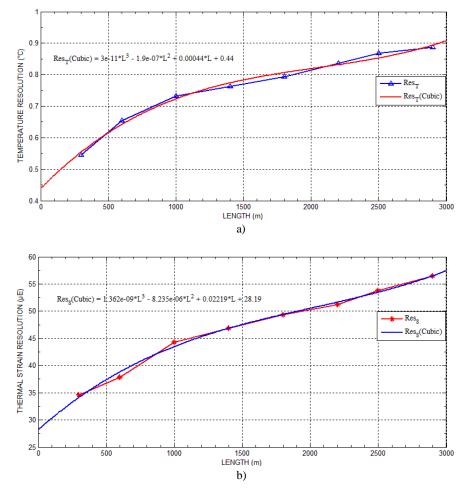

a)

b)

Fig. 8. a) Temperature and b) Thermal strain resolutions

$\triangle VB\ (n) = - 0.00087703*n^2 + 2.358e+05*n - 3.3996e+05$

Fig. 9. Variation of BFS with core refractive index

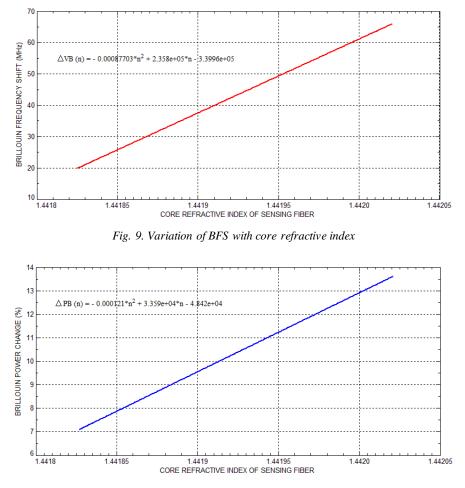$\triangle PB\ (n) = - 0.000121*n^2 + 3.359e+04*n - 4.842e+04$

Fig. 10. Variation of BPC with core refractive index

5. Conclusion

In this study, a novel distributed temperature and thermal strain sensing model depending on the combined effect of the core refractive index and Coherent detection of spontaneous Brillouin scattering has been utilized. Using this model, core refractive index dependencies of BFS and BPC have been mathematically analyzed and corresponding simulations have also been acquired.

For thermal strain and temperature variations of the sensing fiber from 0 µε to 521.635 µε and from 20 °C to 39.44 °C, core refractive index variations have been obtained in range of 1.44183 - 1.44202. Moreover, Brillouin frequency shift RMS and the Brillouin power change RMS profiles have been plotted and both the linear and quadratic equations related to the RMS error values have been derived. Using these equations, average values of the frequency shift RMS and the power change RMS of Brillouin Coherent detection based distributed sensing system have been calculated as ~ 1.60 MHz and ~ 0.26 %, respectively. Furthermore, temperature and thermal strain resolutions have been calculated for specific fiber regions and using the interpolation and curve fitting methods, cubic equations of the resolutions have been obtained. Average values of the temperature and thermal strain

resolutions of the sensing system have been computed from the fitted curves as ~ 0.76 °C and ~ 46.80 µε along the sensing fiber, respectively. Moreover, it is concluded that Brillouin frequency shift RMS is responsible for 10 % of temperature resolution and 67 % of thermal strain resolution, whilst Brillouin power change RMS is responsible for 90 % of temperature resolution and 33 % of thermal strain resolution for this sensing system.

Nevertheless, the quadratic equations with respect to the core refractive index dependencies of the Brillouin parameters have been derived as a function of the fiber length and the corresponding simulations have been performed. It is evidently inferred from the simulations that the linear equations are compatible with the quadratic equations. On the other hand, the quadratic equations give the better solutions compared to the linear equations for getting values of the Brillouin parameters versus the core refractive index values. The core refractive index variation of 1×10^{-5} produces 2.358 MHz variation in BFS, whilst it produces 0.3359 % variation in BPC.

Simulations and equations acquired in this study show that the core refractive index dependencies of the Brillouin parameters can be used as alternatives to other methods relying on spontaneous Brillouin scattering. In other words, in order to evaluate the sensing performance of the

system, valuable temperature and thermal strain information can be obtained by using the core refractive index variations of the sensing fiber.

References

[1] R. Posey, G. A. Johnson, S. T. Vohra, Electron. Lett. **36**(20), 1688 (2000).

[2] A. Masoudi, M. Belal, T. P. Newson, Meas. Sci. Technol. **24**(8), Art. ID 085204, (2013).

[3] F. Peng, Y. J. Rao, Z. N. Wang, Opt. Fiber Commun. Conf. Los Angeles, CA, USA, paper W3I.6 (2015).

[4] Y. Wu, J. Gan, Q. Li, Z. Zhang, X. Heng, Z. Yang, IEEE Photonics Journal **7**(6), 1 (2015).

[5] M. Abbasnejad, B. Alizadeh, IEEE Sensors Journal **18**(5), 2015 (2018).

[6] M. Yucel, H. H. Goktas, M. Yucel, N. F. Ozturk, A. E. Gunduz, Turk J. Elec. Eng. & Comp. Sci. **25**(5), 3881 (2017).

[7] M. Li, W. Jiao, X. Zhang, Y. Song, H. Qian, J. Yu, IEEE Journal of Selected Topics in Quantum Electronics **23**(2), 1 (2017).

[8] M. Alahbabi, Distributed optical fiber sensors based on the coherent detection of spontaneous Brillouin scattering, PhD Dissertation, University of Southampton, (2005).

[9] H. H. Kee, G. P. Lees, T. P. Newson, Optics Letters **25**(10), 695 (2000).

[10] G. Gopalakrishnan, I. M. Serene, R. Jacop, G. Amit, S. K. Sudheer, Z. C. Alex, S. Abraham, S. M. Hardas, A. R. Krishnan, Optoelectron. Adv. Mat. **2**(1), 10 (2008).

[11] P. B. Bansal, R. H. Doremus, Handbook of glass properties, Academic Press, (1986).

[12] K. R. C. P. De Souza, Fiber optic distributed sensing based on spontaneous Brillouin scattering, PhD Dissertation, University of Southampton, (1999).

[13] A. Gunday, S. E. Karlik, G. Yilmaz, J. Optoelectron. Adv. M. **18**(11 – 12), 1000 (2016).

[14] M. Yucel, N. F. Ozturk, Instrumentation Science & Technology, DOI: 10.1080/10739149.2017.1415930, (2018).

[15] T. Horiguchi, T. Kurashima, M. Tateda, IEEE Photonics Tech. Lett. **2**(5), 352 (1990).

[16] Y. Zhang, G. Fu, Y. Liu, W. Bi, D. Li, Optik **124**(8), 718 013).

[17] R. LV, T. Zhou, L. Zhang, H. Peng, Y. N. Zhang, Optoelectron. Adv. Mat. **11**(11-12), 633 (2017).

_____

[*]Corresponding author: agunday@uludag.edu.tr